ELSEVIER

Ceramics International 33 (2007) 337–344

CERAMICS INTERNATIONAL

www.elsevier.com/locate/ceramint

Elaboration and characterisation of apatite based mineral supports for microfiltration and ultrafiltration membranes

S. Masmoudi [a,b], A. Larbot [b], H. El Feki [a], R. Ben Amar [a,*]

[a] *Laboratoire des Sciences de Matériaux et Environnement, Faculté des Sciences de Sfax, route de Soukra Km4, 3018 Sfax, Tunisie*

[b] *Institut Européen des Membranes, UMR 5635 – CNRS, ENSCM, UM II Campus CNRS, 1919 route de Mende, 34293 Montpellier, Cedex 5, France*

Received 24 September 2004; received in revised form 22 July 2005; accepted 4 October 2005
Available online 18 January 2006

Abstract

The development and the characterisation of new supports for microfiltration and ultrafiltration membranes from apatite applied to filtration are presented. The choice of this material is based primarily on its low cost (considering its abundance in the Tunisian ores).

The support, with tubular configuration, was prepared from natural apatite: apatite powders were crushed for 30 min and sieved to 200 μm. The resulting powders, mixed with organic additives and water, could be extruded to elaborate a porous structure. The firing temperature of the support is 1160 °C. The morphologies of the surface and the cross-section observed on scanning electron microscope (SEM) are homogeneous and do not present any macro defects (cracks, etc.). The mean pore diameter, measured by mercury porosimetry, is 6 μm and the pore volume is 48%.

Keywords: A. Extrusion; E. Membrane; Paste characteristic; Porous supports; Apatite

1. Introduction

In most cases, inorganic membranes employed in separation processes are prepared with alumina, titania or zirconia. They are asymmetric and present a composite structure: a porous support which gives the mechanical resistance and thin layers successively deposited on it.

The use of ceramic membrane has advantages such as high thermal and chemical stability, pressure resistance, long lifetime, and catalytic properties from their intrinsic nature [1,2]. Until now, the production of industrial membrane uses a limited choice of materials. As a consequence, the price of ceramic membranes is high and a significant effort was provided in these last years in membrane technology field in order to find new porous ceramic materials [3–5] with clays and apatites. These materials are in abundance and need lower firing temperature than metal oxide materials.

Apatites, present interesting physicochemical properties. So they make it possible in particular to trap heavy or radioactive metals [6–8]. They are also interesting biomaterials [9,10] or used for environmental applications [11–13].

Apatites are often identified by the general formula $M_{10}(XO_4)_6Y_2$, with M: Ca, Sr, Ba, Pb, etc.; X: P, As, Si, etc.; Y: various anions, such as OH^-, F^-, Cl^- or other groups [14–19].

In nature apatites are very abundant; they are found in phosphate mines where they form the principal constituent. In the biological environment, they constitute the major part of the mineral matter of the vertebra skeleton. These apatites are used as a raw material in many processes of chemical industries, such as for the preparation of artificial fertilisers [20], for the manufacture of catalysts or for osseous prostheses [21,22].

Apatite crystallizes in the hexagonal system with the space group $P6_3/m$. The almost compact assembly of orthophosphate ions PO_4^{3-} has two types of tunnel. The narrow one (tunnel I) contains cations localised in site (I) with the symmetry 4f, corresponding to a coordination number of nine and the wider one (tunnel II) with cations in site (II), with the symmetry 6 h, and a coordination number of six or seven. One of the main characteristics of the apatitic structure is to allow various substitutions for both cations and anions [23].

This study is related to the elaboration of porous supports using raw apatite. The choice of this material is based on its low

* Corresponding author. Tel.: +216 98 211 476; fax: +216 74 274 437.
E-mail address: raja.rekik@fss.rnu.tn (R.B. Amar).

0272-8842/$32.00
doi:10.1016/j.ceramint.2005.10.001

temperature of sintering, thermal stability and good chemical resistance particularly to bases.

2. Experimental

2.1. Characterisation of the apatite powder

Apatite powder is coming from Metlaoui in the south of Tunisia. Different techniques were used for the characterisation.

The chemical composition of the apatite powder was determined by spectroscopic techniques, as X-ray fluorescence for metals and by atomic absorption for alkaline earth metals. The loss of ignition was obtained at 1000 °C.

The powder morphology as well as the microstructure of samples were obtained using a HITASHI scanning electron microscope (SEM).

Purity of the apatite powder was tested by IR spectral analysis. An IR transmittance spectrum of the ground sample was obtained in the 4000–400 cm^{-1} range with a SHIMATZU IR 470 spectrometer.

The spectra were taken from thin KBr pellets prepared by compacting an intimate mixture obtained with 1.5 mg of apatite and 300 mg of KBr [24].

Phases present in the powder compositions were analysed using an X-ray diffractometer (Siemens, Germany) with Cu Kα radiation (λ = 0.154 nm).

The apatite particle sizes were calculated on the basis of specific surface areas, measured using a BET surface area analyser (ASAP 2010 MICROMERITIC).

Thermogravimetric analysis (TGA) and differential scanning calorimetry (DSC) (DSC-TGA 2960 de TA Instruments) were carried out with approximately 22 mg of apatite. Temperature varied from 0 to 1000 °C at a rate of 5 °C/min, under air.

The dilatometry study was led with a dilatometer type TMA 92 SETARAM, in a large temperature range under a controlled atmosphere of argon. The dilatometry analysis was carried out with apatite powder at a heating rate of 10 °C/min, from room temperature to 1200 °C.

The characterisation of crude pastes was conducted using a texturometer TEC T04, ETIA. A cone was used for the penetration tests and two successive experiments were conduced. Penetration stress σ_c was calculated from the penetration force F using the following formula [25]:

$$\sigma_c = \frac{F}{\pi E^2 \tan^2 \mu}$$

where E: penetration depth = 30 mm; μ: angle of the cone probe = 15°.

Cohesiveness is defined as the ratio of the compression work during the second cycle over the compression work during the first one; adhesiveness is the area of the feed back curve when the probe moves back to initial position. Elasticity is the ratio of the compression time during the first cycle over that during the second cycle.

2.2. Elaboration of porous support

The elaboration of a ceramic macroporous support implies the following sequence of operations:

- preparation of a plastic ceramic paste;
- shaping by extrusion;
- consolidation by thermal treatment.

In Fig. 1, the process of the ceramic preparation is described.

Elaboration of a synthetic ceramic powder requires a specific ageing and also use organic additives. In general, these additives favour the powder dispersion and the adjustment of the paste rheology. They also ensure a significant mechanical resistance before the final consolidation by sintering. The principal advantage of the organic additives is that they are eliminated by combustion during the thermal treatment.

The optimised composition of the paste is (values are given in wt%):

- apatite powder: 84;
- organic additives: methocel (The Dow Chemical Company): 2.5 amijel (Cplus 12076, Cerestar): 2.5, porosity agent: starch (RG 03408, Cerestar): 9, PEG: 2.

Before the preparation of the paste, the powder was grounded at 250 tr/min during 30 min and sieved at 200 μm. Necessary water for the pugging was added, up to the quantity of 53 ml/200 g of mixed powder.

Before extrusion stage, an ageing stage of the paste is necessary to obtain a good homogeneity and to favour the hydration of the cellulose binders. The time necessary for this stage is 24 h. Shaping was performed by extrusion. The drying of the extruded pieces was conducted in air at room temperature during 24 h. Sintering was performed at a temperature ranging from 1150 to 1200 °C.

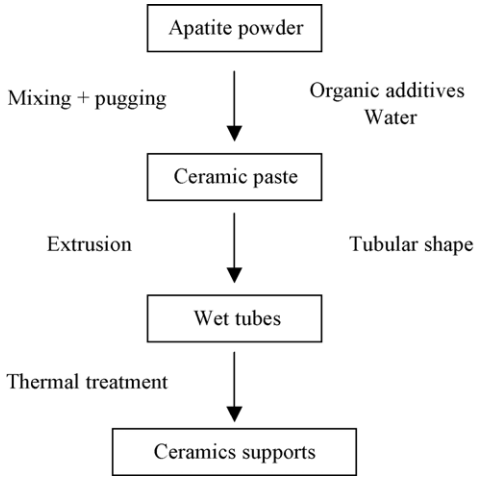

Fig. 1. Various steps of macroporous ceramics preparation.

Table 1
Chemical analysis of apatite powder

	Elements										
	P_2O_5	CaO	SiO_2	Al_2O_3	Fe_2O_3	MgO	CO_2	SO_3	C org	Cl^-	F^-
Wt (%)	28.92	49.14	3.10	0.58	0.26	0.70	0.90	3.21	0.90	0.10	0.10

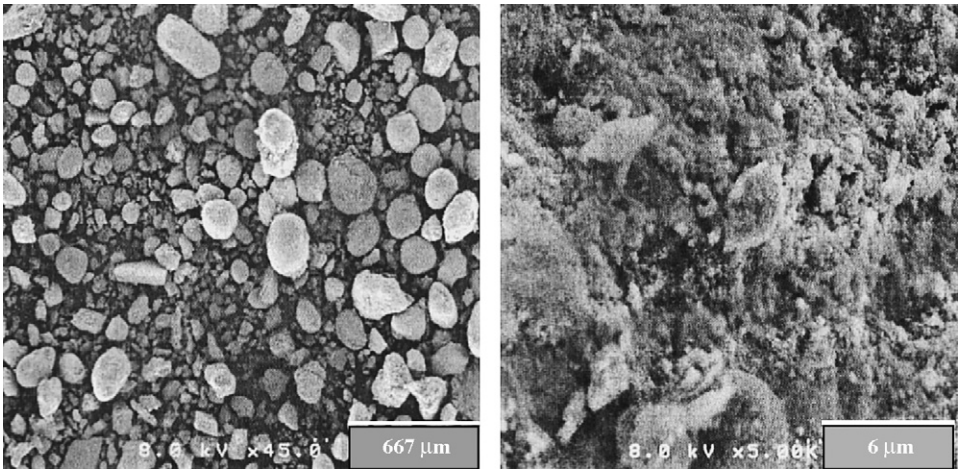

Fig. 2. SEM image of the apatite powder at different magnitudes.

3. Results and discussion

3.1. Characterisation of the apatite powders

The chemical analysis of apatite powder is shown in Table 1. The result shows that the major phase contains calcium and phosphate.

The powder morphology determined by SEM at different magnifications is presented in Fig. 2. The natural apatite has not a particular shape even the grain size distribution remains homogeneous.

The IR spectrum of the sample is shown in Fig. 3. Recorded IR spectrum of the sample shows bands relative to apatite. The bands at 3570 and 630 cm^{-1} are characteristic for stretching and vibrational modes of the OH^- ions respectively [24,25]. The strongest peaks of apatite at 1037, 1110 and 964 cm^{-1} are attributed to PO_4^{3-} [26,27], the peaks at 565 and 607 cm^{-1} were assigned to P-O mode [28]. 469 cm^{-1} band results from the ν_2 phosphate mode [29]. In addition, the bands relative to CO_3^{2-} ions (876–1420–1463 cm^{-1}) are present.

Fig. 4 represents the X-ray diffractogram of the apatite sample. It shows characteristic peaks of apatite. The main phase crystallises in the hexagonal system, in the space group $P6_3/m$ [30].

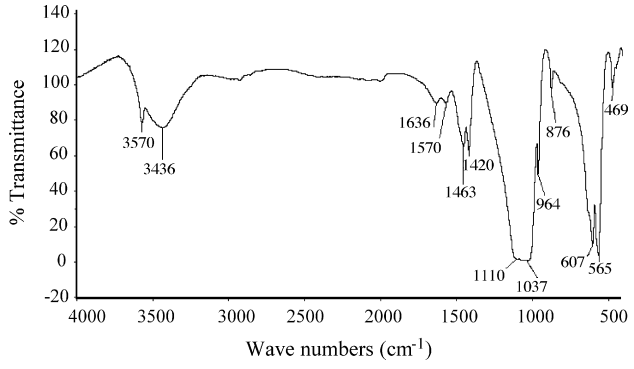

Fig. 3. IR spectrum of the apatite sample.

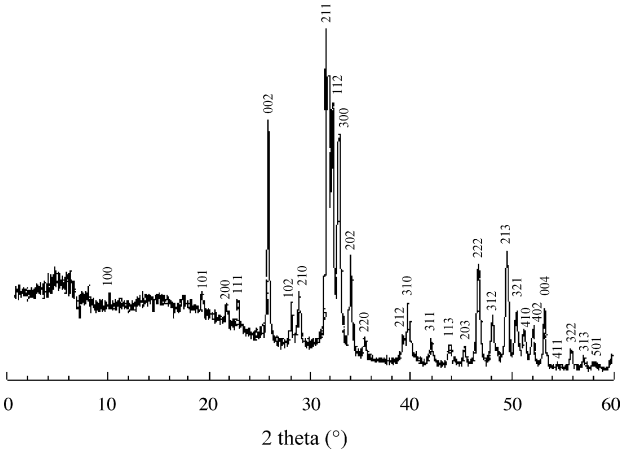

Fig. 4. X-ray diffractogram of the apatite sample.

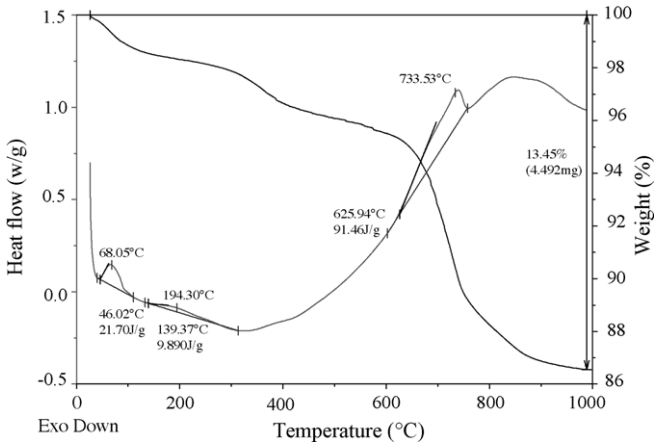

Fig. 5. Thermal analysis curve: DSC and TGA for apatite powder with organic additives.

The BET surface area is 23.16 m^2/g (± 0.06 m^2/g) and the adsorption average pore radius (BET) is in the order of 45.7 Å, value which corresponds to mesopores range.

The DSC-TGA data of apatite powder are represented in Fig. 5. Three endothermic peaks are detected [31]:

- one peak with a significant intensity appears at 68 °C, corresponding to a weight loss of 1.8%. This peak is due to the loss of residual water (moisture);
- one less intense peak which appears at about 194.30 °C, accompanied by a weight loss of 2.2% which corresponds to the dehydration of HPO_4^{2-} ions according to the following reaction:

$$2\,HPO_4^{2-} \rightarrow P_2O_7^{4-} + H_2O \quad (1)$$

- simultaneously the reduction of CO_3^{2-} ions (present in phosphate rock) content occurs, (reaction with ions HPO_4^{2-}) according to the reaction:

$$CO_3^{2-} + 2\,HPO_4^{2-} \rightarrow CO_2 + 2\,PO_4^{3-} + H_2O \quad (2)$$

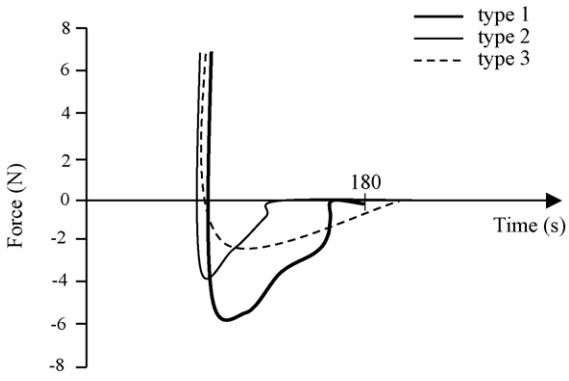

Fig. 7. Evolution of the adhesion force with time.

- another weak intensity peak at about 733.53 °C is accompanied by a weight loss of 9.4%. It is due to the reduction of OH^- and CO_3^{2-} contents following equations:

$$P_2O_7^{4-} + 2\,OH^- \rightarrow 2\,PO_4^{3-} + H_2O \quad (3)$$

$$P_2O_7^{4-} + CO_3^{2-} \rightarrow 2\,PO_4^{3-} + CO_2 \quad (4)$$

Another peak at 319.6 °C was obtained during the analysis of apatite powder with organic additives. The three peaks already described are related to natural apatite and apatite with organic additives. The new peak corresponds to the elimination of added organic materials.

For the dilatometry analysis, the time–temperature sintering profile used in the experiments is given in Fig. 6. The shrinkage, which attains about 20%, begins at about 700 °C.

3.2. Characterisation of the ceramic paste

The negative peak obtained during the extraction of the cone provided various information on the adhesion, the elasticity and

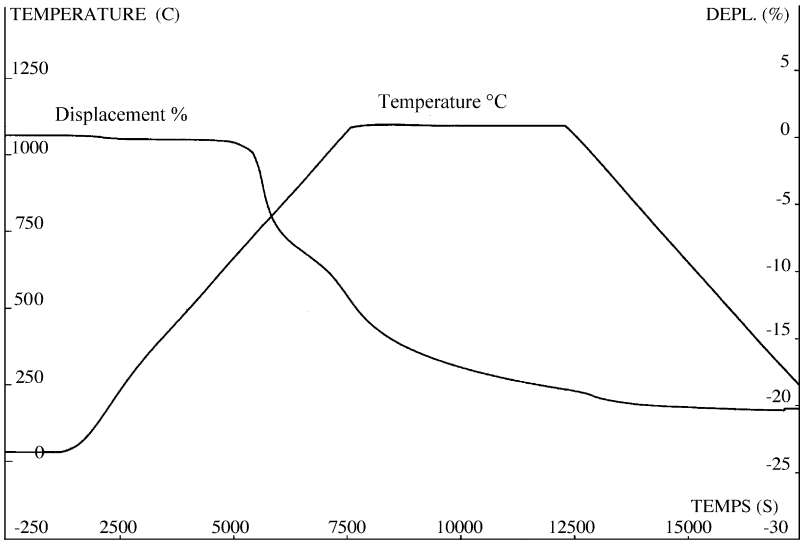

Fig. 6. Dilatometry analysis curve.

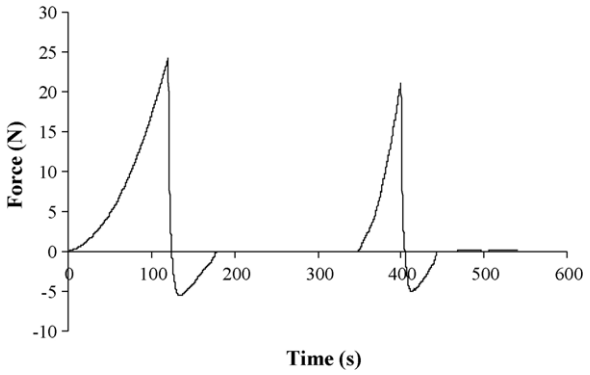

Fig. 8. Evolution of the force applied vs. time.

the plasticity of the paste. We observe three types of peaks (Fig. 7). The decreasing part of the curve and the value of the minimum are related to the hardness of the paste. The increasing part of the negative peak shows different properties according to the profile type:

- Profile type 1: the main characteristic of this profile is the discontinuity observed at the end of the probe ascent. This indicates that the deformation and the plasticity degree of the paste are conserved.The curve inflection observed between the minimal value and the break can be related to the paste elasticity degree.
- Profile type 2: we observe a continuous evolution of the force (with an inflection point), during the withdrawal of the cone. This behaviour is observed with intermediate hard pastes, not much sticking and not much plastic. Such deformation curve can be related to the elastic character of the paste.
- Profile type 3: in this last case, there is no inflection in the evolution force during the withdrawal of the cone. This is due to the very adhesive character of the paste.

In our case (profile type 2, Fig. 8), a continuous evolution of the force (with an inflection point) during the withdrawal of the cone is noted. This behaviour is observed with harder pastes that are not sticking and not plastic. This regular deformation of the paste can be due to its elastic character.

Cohesiveness, adhesiveness and elasticity were also recorded (Table 2).

The increase of σ_{c1} and σ_{c2} with the ageing time (Table 2) corresponds to the increase of the hardness of the paste and results are presented in Fig. 9. It is noted that the values of the cohesiveness and adhesiveness after an ageing time of 0 and 48 h are very similar. At these ageing times, pastes lose their necessary extrusion characteristics. Thus, a 24 h ageing time was chosen.

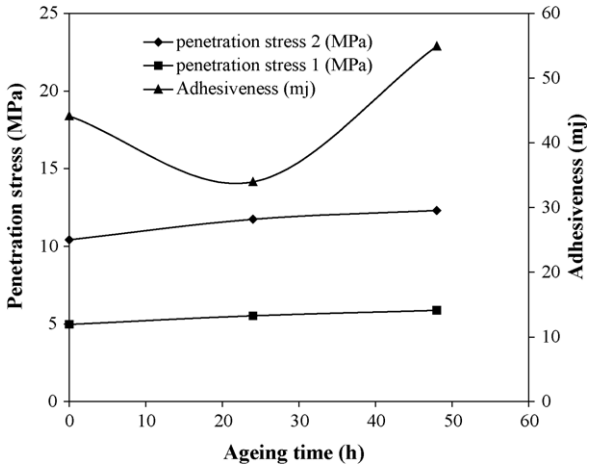

Fig. 9. Evolution of the textural parameters against the ageing time of paste.

3.3. Characterisation of the membrane supports

3.3.1. Scanning electron microscopy (SEM)

The micrographs relating to the evolution of the microstructure of apatite membranes with the increasing sintering temperature are shown in Fig. 10. It can be seen the surface of tubular supports sintered at temperatures ranging from 1100 to 1220 °C.

Below 1150 °C, we detect the presence of intergranular contacts which are large enough to ensure the ceramics cohesion (beginning of sintering).

We observe that the formation of grain boundaries is achieved within a narrow temperature range of 1150–1170 °C. The aspect of the surface is homogeneous and does not present any macro defect (cracks, etc.). We also observe the occurrence of a smooth surface with a low roughness, which will be able to allow the deposit of a homogeneous layer.

Beyond 1180 °C, the densification process (shrinkage) dominates and a relatively open structure is still observed.

3.3.2. Mercury porosimetry

The evolution of support characteristics (pore diameter and pore volume) is presented in Fig. 11. We note that the average pore diameter decrease with the ageing time. However, the porous volume increases for 24 h ageing and decrease slightly for 48 h ageing, to attain a value of 41%.

The evolution of the average pore diameter, dp (μm) and of the pore volume, vp (%), against the temperature of sintering reveals that vp decreases from 50 to 45% between 1150 and 1200 °C, while dp increasing from 5 to 8 μm (Fig. 12). In the 1150–1170 °C temperature range, ceramics presents a dp value

Table 2
Values of the textural paste parameters (F: penetration force; σ_c: penetration stress; C: cohesiveness; A: adhesiveness; E: elasticity)

Ageing time (h)	$F1$ (N)	$F2$ (N)	σ_{c1} (MPa) × 10^4	σ_{c2} (MPa) × 10^4	C	A (mJ)	E
0	24.22	21.15	11.930	10.421	0.413	44.15	2.36
24	26.95	23.83	13.275	11.742	0.382	33.96	2.47
48	28.64	25	14.108	12.315	0.402	54.95	2.70

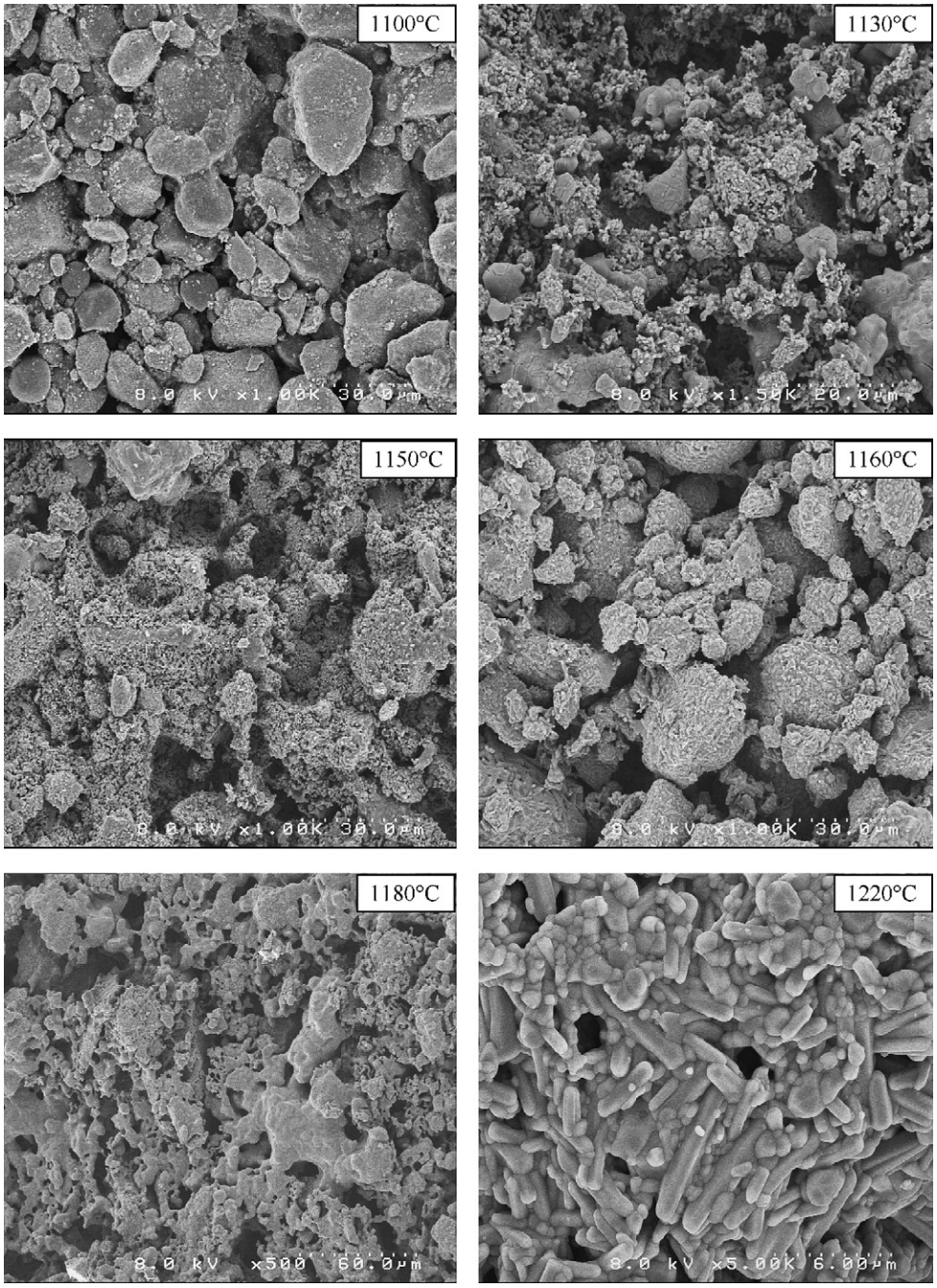

Fig. 10. Micrographs (SEM) of internal surface of tubular supports at various sintering temperature.

of 5–6 μm with an average porosity of 48%. This high porosity value is a necessary condition to ensure a negligible flow resistance during microfiltration.

3.3.3. Mechanical resistance

The measurement of the mechanical resistance of supports was carried out by the three point bending method (LLOYD Instrument) applied to sintered parallelepipedic test bars. The size of samples was 40 mm × 10 mm × 2 mm. Crosshead speed used was 0.25 mm/s and the width between supports is 24 mm. Fig. 12 shows the evolution of the maximum fracture stress, σ (MPa), according to the temperature, using a sintering temperature range between 1150 and 1180 °C. The increase of σ with the temperature indicates a progressive increase in the material mechanical resistance. Furthermore, sintering above 1200 °C does not increase the mechanical resistance. This result agrees with the texture observation by SEM and it is comparable with other observations obtained with membrane support manufactured with Moroccan clay [32].

3.3.4. Corrosion resistance

The support, sintered at 1160 °C, was soaked at 80 °C using nitric acid and soda solutions. The pH was equal to 1 and 13, respectively. The results reported on Fig. 13 shows that apatite

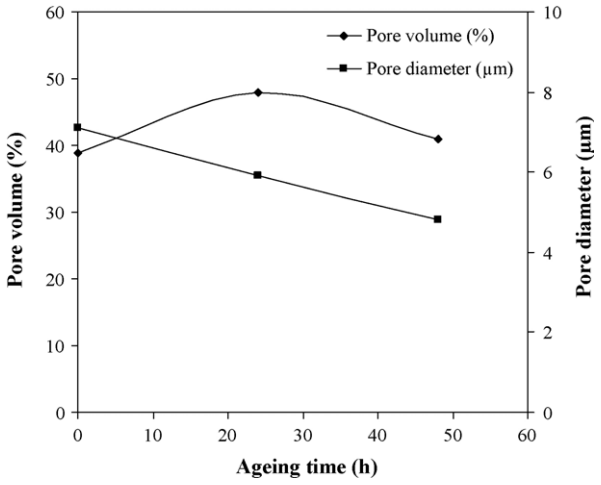

Fig. 11. Variation of pore diameter and pore volume as a function of ageing time of the paste.

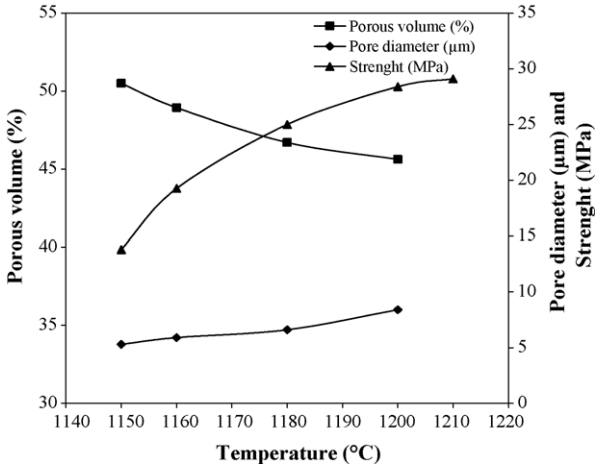

Fig. 12. Variation of pore diameter, pore volume and mechanical resistance as a function sintering temperature.

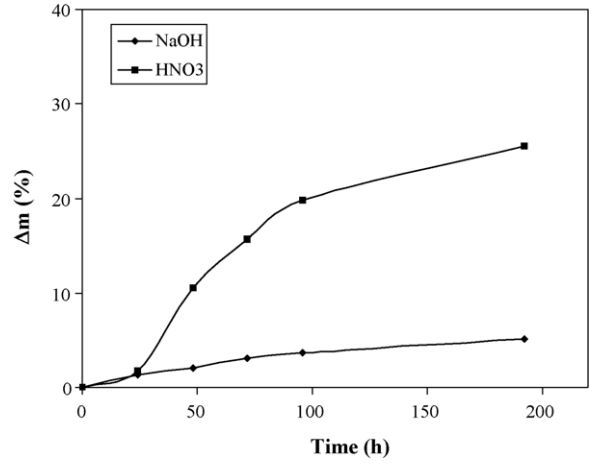

Fig. 13. Weight loss of support in nitric acid and soda solutions at 80 °C as a function of time.

supports resist better in basic medium than in acid medium: The weight loss does not exceed 5 wt% in 8 days at pH 13. However, in acid medium (pH 1), the weight loss exceeds 25 wt%. These results are comparable with those presented by El Moudden et al. [32] especially in basic medium. However, in acid medium, supports made with clays have a better resistance than those from apatite. The weight loss attains 6 wt% at 40 °C and 20 wt% at 80 °C.

4. Conclusions

This study reports the development and the characterisation of new tubular supports based on sintered natural apatite. They can be used for tangential microfiltration and ultrafiltration.

The analysis of the material powder confirmed the presence of the apatite structure. The choice of the paste composition and of the sintering temperature favours the increase of the mechanical resistance while maintaining an important porous volume (porosity greater than 40%) as well as a good chemical resistance essentially in basic solution.

The obtained ceramic support has a mean pore diameter of about 6 μm with an average porosity of 47%.

Then, apatite materials are appropriate for the development of membranes supports for microfiltration or ultrafiltration that can be applied at pH >4 for the industrial liquid waste processing.

References

[1] A. Larbot, J.P. Fabre, C. Guisard, L. Cot, J. Gillot, New inorganic ultrafiltration membranes: titania and zirconia membranes, J. Am. Ceram. Soc. 72 (1989) 257–261.
[2] M.A. Anderson, M.J. Gieselmann, Q. Xu, Titania and alumina ceramic membranes, J. Membr. Sci. 39 (1988) 243–258.
[3] A.S. Mukasyan, C. Costello, K.P. Sherlock, D. Lafarga, A. Varma, Perovskite membranes by aqueous combustion synthesis: synthesis and properties, Sep. Purif. Technol. 25 (2001) 117–126.
[4] S. Chemlal, M. Sghyar, M. Rafiq, A. Larbot, L. Cot, Elaboration de membranes de spinelles de cobalt $CoAl_2O_4$ et de spinelle de manganèse $MnAl_2O_4$ pour l'ultrafiltration, Ann. Chim. Sci. Mat. 25 (2000) 577–582.
[5] Y. Li, X. Zhang, J. Wang, Preparation for ZSM-5 membranes by a two-stage varying-temperature synthesis, Sep. Purif. Technol. 25 (2001) 459–466.
[6] Y. Takruchi, T. Suzuki, H. Arai, A study of equilibrium and mass transfer in processes for removal of heavy-metal ions by hydroxyapatite, J. Chem. Eng. Jpn. 21 (1988) 98–100.
[7] Q.Y. Ma, S.J. Traina, T.J. Logan, J.A. Ryan, In situ lead immobilisation by apatite, Environ. Sci. Technol. 27 (1993) 1803–1810.
[8] T. Suzuki, T. Hatsushika, M. Miyake, Synthetic hydroxyapatites as inorganic cation exchangers. Part 2, J. Chem. Soc., Faraday Trans. I 78 (1982) 3605–3611.
[9] H. Aoki, Science and Medical Applications of Hydroxyapatite, Takayama Press, Tokyo, 1991.
[10] K. De Groot (Ed.), Bioceramics of Calcium Phosphate 99114, CRC Press, Boca Raton, FL, 1983.
[11] C. Rey, Calcium Phosphates in Biological and Industrial Systems, Kluwer Academic Publishers, London, 1998.
[12] T.A. Ioannidis, A.I. Zouboulis, Detoxification of a highly toxic lead-loaded industrial solid waste by stabilization using apatites, J. Hazardous Mater. 97 (2003) 173–191.
[13] F.Z. Boujrhal, J. Carpena, R. Cherkaoui El Moursli, A. Chouak, study of radon retention and fission track annealing with temperature in natural apatite, Radiat. Phys. Chem. 61 (2001) 645–647.

[14] J.R. Van Wazer, Phosphorus and its Compounds Chemistry, vol. 1, Interscience, New York, 1958.
[15] A. Nounah, J.L. Lacout, J.M. Savariault, Localization of cadmium in cadmium-containing hydroxy- and fluorapatites, J. Alloys Compd. 188 (1992) 141–146.
[16] J.C. Elliot, J. Am. Ceram. Soc., Structure and Chemistry of the Apatites and other Calcium Orthophosphates, Elsevier, Amsterdam, 1994.
[17] M. Azzour, Doctoral thesis, University of Rabat, Morocco, 1998.
[18] M. Azzour, L. El Ammari, Y. Le Fur, B. Elouadi, Etude structurale d'orthovanadates d'alcalins et de plomb cristallisant avec la structure apatite lacunaire, J. Solid State Chem. 141 (1998) 373–377.
[19] D.E.C. Corbridge, Topics in Phosphorus Chemistry, 3, Wiley, New York, 1966.
[20] A. Pagnoul, Note relative à l'emploi des phosphates dans les engrais, Annales agronomiques 5 (1879) 358–365.
[21] M. Jarcho, Calcium phosphate ceramics as hard tissue prosthetics, Clin. Orthop. Rel. Res. 157 (1981) 259–269.
[22] H. Aoki, Science and Medical Application of Hydroxyapatite, Takayama Press, Tokyo, 1991, p. 1.
[23] D. Mc Connel, Apatites, Springer, New York, 1973.
[24] R.N. Hannah, J.S. Swinehart, Experiments in techniques of infrared spectroscopy, Pekin-Elmer, ed. Norwalkonn, 1974.
[25] J. Benbow, Paste Flew and Extrusion, Oxford University Press Inc., New York, 1993.
[26] D.W. Halcomb, R.A. Young (Eds.),Thermal decomposition of human tooth enamel and calcif Tissue Int. 31 (1980) 189.
[27] K. Kandori, N. horigami, A. Yasukawa, T. Ishikawa, J. Am. Ceram. Soc. 80 (1997) 1157.
[28] S.J. Joris, C.H. Amberg, J. Phys. Chem. 75 (1971) 3172.
[29] B.O. Fowler, Infrared spectra of apatite, in: W.E., Brown, R.A., Young (Eds.), International Symposium on Structural Properties of Hydroxyapatite and Related Compounds, Gaithersburg, MD, 1968 (Chapter 7).
[30] M. Mehmel, Z. Kristallogr. 75 (1930) 323.
[31] E. Landi, A. Tampieri, G. Celotti, L. Vichi, M. Sandri, Influence of synthesis and sintering parameters on the characteristics of carbonate apatite, Biomaterials 25 (10) (2004) 1763–1770.
[32] N. El Moudden, A. Elghazouali, S. Rakib, M. Sghyar, M. Rafiq, A. Larbot, L. Cot, Nouveaux supports membranaires à base de chamotte d'argile, Ann. Chim. Sci. Mat. 26 (2) (2001) 5–11.